

Transparent SiO₂-Ag core-satellite nanoparticle assembled layer for plasmonic-based chemical sensors

Tsung-Han Chen, Ren-Der Jean, Kuo-Chuang Chiu, Chun-Hua Chen, and Dean-Mo Liu

Citation: *Applied Physics Letters* **100**, 223101 (2012); doi: 10.1063/1.4722583

View online: <http://dx.doi.org/10.1063/1.4722583>

View Table of Contents: <http://scitation.aip.org/content/aip/journal/apl/100/22?ver=pdfcov>

Published by the *AIP Publishing*

Articles you may be interested in

[Maximizing surface-enhanced Raman scattering sensitivity of surfactant-free Ag-Fe₃O₄ nanocomposites through optimization of silver nanoparticle density and magnetic self-assembly](#)

J. Appl. Phys. **114**, 124305 (2013); 10.1063/1.4823732

[Controlling the absorption spectrum within a thin amorphous silicon layer by using the size dependent plasmonic behaviour of silver nanoparticles](#)

J. Renewable Sustainable Energy **5**, 031614 (2013); 10.1063/1.4809787

[Guided-mode-resonance-coupled plasmonic-active SiO₂ nanotubes for surface enhanced Raman spectroscopy](#)

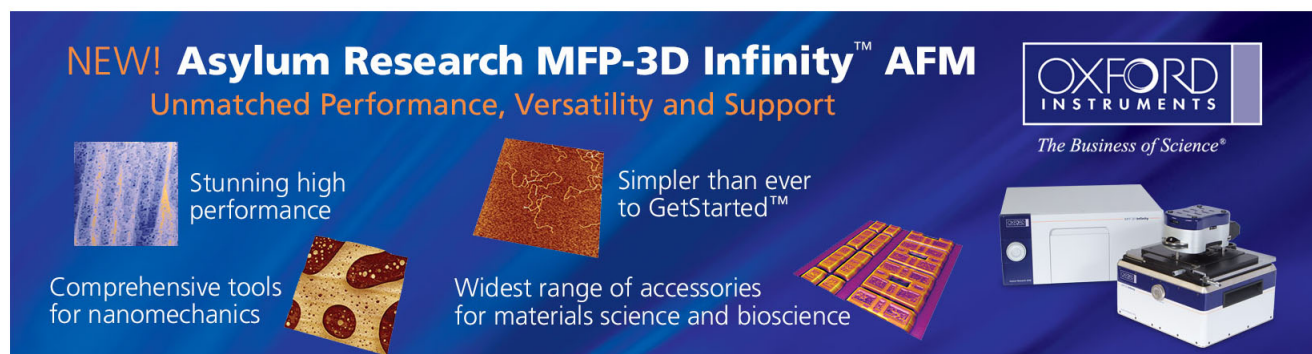
Appl. Phys. Lett. **100**, 191114 (2012); 10.1063/1.4714710

[In situ optical microspectroscopy approach for the study of metal transport in dielectrics via temperature- and time-dependent plasmonics: Ag nanoparticles in SiO₂ films](#)

J. Chem. Phys. **134**, 054707 (2011); 10.1063/1.3537736

[Strategies for nanoplasmonic core-satellite biomolecular sensors: Theory-based Design](#)

Appl. Phys. Lett. **95**, 193112 (2009); 10.1063/1.3254756

The advertisement features a dark blue background with white and orange text. At the top left, it reads 'NEW! Asylum Research MFP-3D Infinity™ AFM' in large white letters, followed by 'Unmatched Performance, Versatility and Support' in orange. On the right, the Oxford Instruments logo is shown with the tagline 'The Business of Science®'. Below the text are several images: a blue textured surface, a brown textured surface, a grid of colorful squares, and the physical AFM instrument. Text boxes describe the instrument's capabilities: 'Stunning high performance', 'Simpler than ever to GetStarted™', 'Comprehensive tools for nanomechanics', and 'Widest range of accessories for materials science and bioscience'.

Transparent SiO₂-Ag core-satellite nanoparticle assembled layer for plasmonic-based chemical sensors

Tsung-Han Chen,^{1,a)} Ren-Der Jean,^{1,a)} Kuo-Chuang Chiu,² Chun-Hua Chen,^{1,b)} and Dean-Mo Liu^{1,b)}

¹Department of Materials Science and Engineering, National Chiao Tung University, Hsinchu 300, Taiwan

²Material and Chemical Research Laboratories, Industrial Technology Research Institute, Hsinchu 310, Taiwan

(Received 1 March 2012; accepted 3 May 2012; published online 29 May 2012)

We discovered a promising sensing capability of SiO₂@Ag core-satellite nanoparticles with respect to organic melamine when they were consolidated into a solid-type thin-film entity. A series of theoretical models were proposed which provided calculation outcomes superior to those of existing models for the localized surface plasmon resonance spectra of the solid-state assemblies. We envisioned not only that such a SiO₂@Ag film is a potential candidate for a transparent solid-state optical nanosensor for the detection of organic molecules but also that the resulting plasmonic resonance model facilitates a better understanding of such a solid-state nanosensor used for a number of sensory applications. © 2012 American Institute of Physics. [<http://dx.doi.org/10.1063/1.4722583>]

Metallic nanostructures including isolated quantum crystals with zero to three dimensions as well as their assemblies have become very attractive in recent years due to their distinct structurally and environmentally dependent optical properties: the so-called localized surface plasmon resonance (LSPR).¹⁻³ The LSPR phenomenon, which exhibits a pronounced absorption band in the UV-visible spectrum, originates from a collective oscillation of the free electrons at the interface between the metals and the dielectric medium with the incident electromagnetic fields. Thus, the wavelength and profile of the absorption bands not only strongly depend on the composition, size, shape, and pattern of the nanostructures but are also extremely sensitive to the dielectric surroundings. These features allow direct detection of analyte binding or a slight dielectric change in the medium containing the analytes in real time and have been applied in a variety of fields including surface enhanced Raman spectroscopy (SERS),^{4,5} biosensing,⁶⁻⁸ and nanolithography^{9,10} and as probes in scanning near-field optical microscopy.^{11,12}

Among these advanced applications, LSPR-based sensors are most promising since they are more accurate than sensors that operate using different principles.^{13,14} In the case of liquid-state LSPR sensors, while the metal nanoparticles adsorb analytic molecules, the interparticle distances change rapidly and thus bring a drastic color transformation due to the near-field electromagnetic coupling.¹⁵ Noble metal nanoparticles such as Au and Ag have been expected to realize highly sensitive detection of target molecules.¹⁶⁻¹⁸ Particularly, Li *et al.* reported that surface-modified Ag nanoparticles used as liquid-state colorimetric sensors could reliably detect melamine and tryptophan to ppm level.^{19,20}

In contrast to the liquid-state sensors, solid-state sensors are generally constructed with orderly or randomly assembled nanocrystals in which all the nanocrystals adhere to substrates.

In such cases, target molecules can also be detected from the LSPR peak shift induced by changes in the dielectric constant of the local nanoparticle surfaces as well as in that of the medium. Many assembly methods, for example, polystyrene nanosphere lithography and nano-imprint technology, have been developed for the preparation of periodic nanostructured films for solid-state sensors.^{21,22} These techniques can be used to form uniform nanostructures to promote reproducibility of LSPR spectra. In particular, Abargues *et al.* reported in which Ag nanoparticles were synthesized *in situ* within PVA films by a one-step procedure.²³ By this method, the LSPR peak position and bandwidth can be tuned to meet the requirements of different targets and to enhance the sensor performance by controlling the shape, size, and spacing of nanoparticles and also the film thickness.

SiO₂@Ag satellite nanoparticles were prepared by the modified Stöber method with the addition of colloidal Ag nanoparticles and were applied as liquid-state sensors for the sensing of organic molecules as described in our previous paper.²⁴ Since it is believed that the sparing distribution of the silver nanoparticles on the silica matrix allows a stable and improved resolution/precision of the emission spectrum, forming a solid-state sensor based on assembly of the SiO₂@Ag nanoparticles should provide additional advantages compared to its liquid-state version, such as ease of handling/carrying, freedom from the colloidal stability issue, and high potential for integration with electronic or optical detection devices. In the meantime, the satellite silver nanoparticles around the silica matrix avoid optically undesirable aggregation since they are well anchored and separated by the silica matrix.

In this work, a solid-state sensor was prepared by assembling the core-satellite nanoparticles into a transparent thin film. We further present a series of experimental results on the UV-vis absorption spectra of the LSPR sensing platform consisting of the SiO₂@Ag satellite nanoparticles and the corresponding theoretical calculations. In addition, the sensing behavior of the solid-state sensors toward melamine molecules will be demonstrated.

^{a)}T.-H. Chen and R.-D. Jean contributed equally to this work.

^{b)}Authors to whom correspondence should be addressed. Electronic addresses: chunhuachen@mail.nctu.edu.tw and deanmo_liu@yahoo.ca.

The SiO₂@Ag nanoparticles for use as solid-state sensors were synthesized by the modified Stöber method with the addition of colloidal silver nanoparticles.²⁴ In brief, in a single reaction vessel, we initially added the follow reagents: 2 mL of tetraethyl-orthosilicate (TEOS) for synthesis, 100 mL of absolute ethanol, 8 mL of ammonia 14%, and 10 mL of deionized (DI) water; all the reactants were mixed by stirring at 300 rpm with a magnetic stir bar at different temperatures from 25 to 75 °C. Then the pH of the solution was controlled in the range of 10.5–11.2. Then 0.892 g of sodium hydroxide (NaOH), 30 mL of ethanol, 30 mL of silver nitrate, and 100 mL of DI water were added to form a final solution at a pH controlled in the range of 9.2–10. The prepared SiO₂@Ag nanoparticles were washed repeatedly with DI water and then re-suspended in ethanol for the subsequent drop-coating on glass substrates. The coated substrates were carefully air-dried at room temperature to obtain a series of homogenous yellow films which were thin enough to be transparent to UV and visible lights. The morphology and particle size of the silica and silver were analyzed using a JEOL JEM-2100F field emission transmission electron microscope (FE-TEM) operated at 200 kV. The morphology of the stacked SiO₂@Ag nanoparticles was analyzed using a JEOL JSM-6700F field emission scanning electron microscope (FE-SEM). The UV-vis absorption spectra were obtained using a Thermo Scientific Evolution 600 spectrometer.

The targeted analyte of melamine (Aldrich, 99%) was dissolved in DI water for the preparation of standard aqueous solutions of 0.1, 1, 10, 100, and 1000 ppm for the subsequent sensing measurements. The SiO₂@Ag thin films were respectively immersed into each standard melamine solution. After 1-h reaction and stabilization time in the melamine solutions, the analyte-reacted films were dried again, and the LSPR peaks were repeatedly recorded using a UV-vis absorption spectroscopy in the range of 300–1000 nm.

Figure 1 shows the morphology of the core–satellite (SiO₂@Ag) nano-objects with the satellite Ag nanoparticles, 5 nm in size on average, around the silica matrix. The silica carrier has an average diameter of 20 nm, and the average distance between adjacent silver nanoparticles is about 5 nm, which is about the same size as the silver nanoparticles. This separation should minimize the effect of interparticle coupling on spectral variation due to adsorption of organic analytes onto the silver nanosensors.

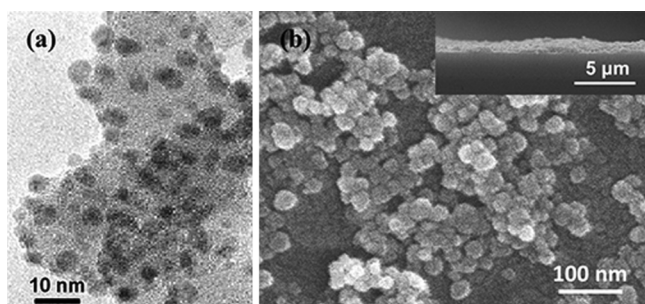


FIG. 1. (a) TEM image: satellite Ag nanoparticles with average diameters of 5 nm around a spherical silica matrix formed so-called core–satellite SiO₂-Ag nanoparticles. (b) Top-view SEM image of the core–satellite SiO₂-Ag nanoparticles stacked on glass substrate. The inset is the cross-sectional SEM image.

However, a closer look at the same TEM micrograph [Fig. 1(a)] clearly reveals a closer contact of the Ag nanoparticles when the core–satellite nano-objects are aggregated to form a solid-state thin-film type sensor in this case. As mentioned above, such an Ag–Ag contact may exert an emitting interference with the resulting surface plasmonic effect, which may risk affecting the accuracy of measurements. To minimize such a potential interference, we aimed to reduce the resulting film thickness, and therefore the thin-film sensor prepared in this work had an average thickness of 1 μm, as illustrated in the inset of Fig. 1(b), with an average of 50 layers of the core–satellite nano-objects being deposited on the glass slides using a drop-coating technology. The resulting thin-film sensors also showed a transparent appearance, which facilitates subsequent optical characterization.

For the purpose of comparison, the present study employed SiO₂@Ag nanoparticle colloids and their assembled thin films as liquid-state and solid-state optical nanosensors, respectively. Different concentrations of melamine of 0.1, 1, 10, 100, and 1000 ppm were used as the target analyte in this test. The traceable change in the LSPR peak was monitored by UV-vis spectroscopy. Figure 2(a) shows the shifts of the LSPR peaks depending on the melamine concentration for both liquid-state and solid-state SiO₂@Ag nanosensors.

For the liquid-type sensor, a slight red shift of about 2 nm can be found for 0.1 ppm melamine aqueous solution. With a further increase in the melamine concentration up to 1000 ppm, a maximum red-shift of about 13 nm can be achieved. Compared with the liquid-type sensor, the solid-state sensor exhibits a much higher sensitivity to melamine molecules. Due to the very low Ag filling ratio, the higher sensitivity does not originate from the coupling effect of the neighboring Ag nanoparticles, as the thin-film configuration was designed to minimize the coupling effect. However, the solid-state sensors indeed show a clear red-shift of 4 nm with 0.1 ppm melamine, indicating that the sensing limit may reach a much lower concentration. A much higher red-shift of about 44 nm with a corresponding melamine concentration of 1000 ppm also means that the concentration of target

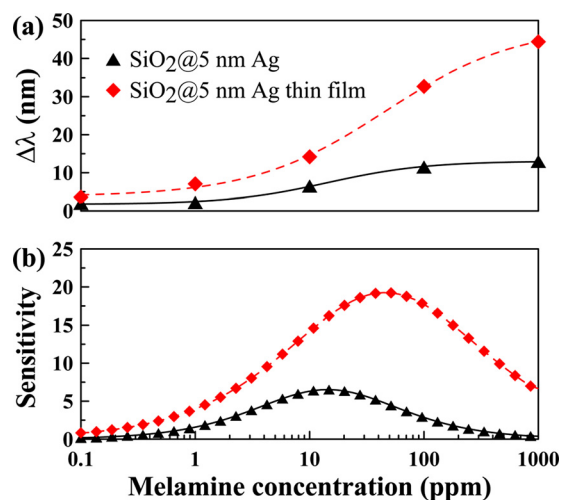


FIG. 2. (a) Melamine-concentration-dependent LSPR peak shifts for the liquid-type and solid-type SiO₂@Ag nanosensors. (b) Differential plots derived from (a).

analyte can be accurately determined. In comparison with the liquid-state version, the currently prepared solid-state nanosensor showed a detection resolution for small organics such as melamine that was 2–4 times higher over the range of concentrations studied.

The sensitivity η of the present Ag LSPR sensors can also be defined as

$$\eta = \frac{\Delta\lambda}{\Delta C}, \quad (1)$$

where $\Delta\lambda$ and ΔC represent the LSPR shift and the change in melamine concentration, respectively. The sensitivity derived from the differential plot of Fig. 2(a) is given in Fig. 2(b), where a strong dependence of the sensitivity on the melamine concentration can be clearly observed for these two nanosensors. The derivative peak top for the solid-state sensor is about three times higher than that for the liquid one. Figure 2(b) clearly shows the better sensitivity of solid-state sensors over the concentration range studied. In addition, the peak position also suggests a suitable concentration range that can be well differentiated with the best resolution for the melamine molecule.

Neglecting the interparticle coupling effect, it is believed that in solid-state configuration, the effect of the surroundings, that is, the dielectric medium, will be minimized due to the removal of highly dielectric liquid, such as water, resulting in a better resolution and sensitivity of the exposed Ag nanoparticles toward the adsorption of molecular melamine. Once adsorbed, the melamine molecules should be well solvated with water as a result of hydrogen bonding between the amino groups of the melamine and the hydroxyl group of water. Such a dielectric solvation is likely to cause a large interference in the plasmonic resonance of the “solvated” surface, resulting in a reduction of the SPR effect. In contrast, without the dielectric medium and solvation of melamine, that is, in a dried configuration, the melamine would lie completely upon the surface of Ag nanoparticles, creating a more compact solid layer without physical and chemical interference from the surroundings. This more compact adsorption layer of melamine may result in a more efficient charge transfer to or interaction with the underlying Ag nanoparticles, leading to a higher responsiveness and sensitivity of the solid-state entity.

A theoretical consideration of the SPR effect of the core–satellite nanoparticle assembled solid-state sensor is important to give a better understanding of how the dielectric surroundings included the air and silica matrix in such a thin-film structure, which will remodel the existing theories on predicting the optical behavior with higher accuracy.

In the liquid state, the Ag nanoparticles were isolated by the SiO₂ matrix and dielectric medium. Thus, the SiO₂@Ag nanoparticles thin-film could be regarded as well-suspended Ag nanoparticles in the silica medium when they were deposited on the glass substrate. Based on the HRTEM observations [Fig. 1(a)], for the subsequent calculations we assumed that the size, distribution, and stack of SiO₂ supporters as well as Ag nanoparticles were ideally uniform with specific values within the sensors. Figure 3(a) (i) show a simplified solid-state SiO₂@Ag sensor for the purpose of

explaining the model only. By neglecting a small population of interparticle contact points within the thin-film structure, it can be assumed that all the Ag nanoparticles were well separated by the SiO₂ matrix. In addition, because the interparticle distance between Ag nanoparticles was comparable to the size of the Ag nanoparticles, here we simply treat the deposited Ag nanoparticles as isolated ones. The classical Mie theory is the simplest theory for modeling the optical properties of small particles,²⁵ and the theoretical formulas are shown in Ref. 26. Figure 3(b) shows the measured and the Mie-calculated UV-vis spectra of the SiO₂@Ag nanoparticles film. Compared with the measured spectrum, the calculated LSPR peak (red-dash line) shows a blue-shift, a slight narrowing of the peak width, and a lower absorption in the lower wavelength region, which should arise from the presumed absence of SiO₂ matrix in this simplified model.

From the measured LSPR spectrum of pure SiO₂ nanoparticle film prepared by the same method as the SiO₂@Ag one [Fig. 3(b)], a mixture of SiO₂ and Ag nanoparticles,

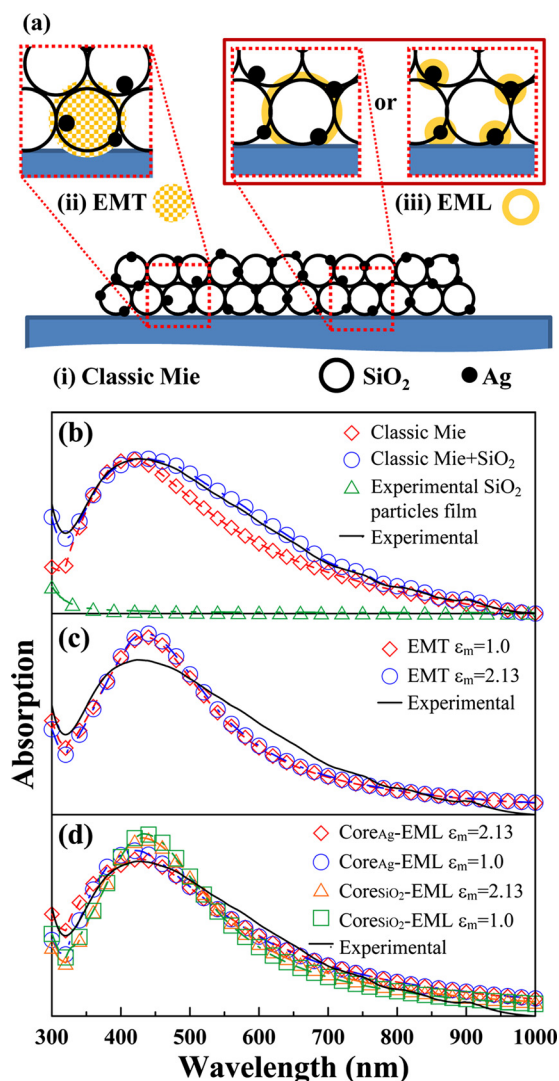


FIG. 3. (a) Sketch of (i) classic Mie theory with mixture model, (ii) EMT model, and (iii) core-EML model constructed for the spectrum calculation of solid-state SiO₂@Ag nanoparticles deposited on glass substrates. (b) Experimental and calculated absorption spectra of classic Mie theory with mixture model. (c) EMT of Ag and SiO₂ nanoparticles model. (d) core-EML model for the SiO₂@Ag nanoparticle film.

instead of the satellite SiO₂@Ag ones, was considered. The experimental spectrum of SiO₂@Ag can thus be fitted with the summation of the individual spectra of Ag nanoparticles (calculated) and SiO₂ nanocarriers (experimental) with specific fractions. The calculated spectra were nicely consistent with the experimental spectra [Fig. 3(b)], indicating that this approach is applicable to the present system.

Although the measured LSPR spectra can be fitted well with the mixture model of isolated SiO₂ and Ag nanoparticles as mentioned above, here we also demonstrated another approach considering a single satellite SiO₂@Ag model due to the unique distribution of particles in the present case. The single satellite SiO₂@Ag model can simplify and speed up the procedure of data analysis. However, uniformity of the prepared specimen is relatively critical to allow an excellent fitting to be obtained by use of such a calculation. In our case, the excellent colloidal stability of the SiO₂@Ag nanoparticles ensures, to a certain extent, the resulting uniformity of deposition, which may facilitate subsequent modeling of the experimental spectral variation.

For the metal–insulator nanocomposites, we took the inhomogeneous matrix–nanoparticle system of SiO₂@Ag as a single homogeneous particle by applying the Maxwell-Garnett effective medium theory (EMT).^{26,27} Figure 3(a) (ii) shows the corresponding EMT model of SiO₂@Ag nanoparticles. For a given dielectric constant of the medium, the fitted curve for the SiO₂@Ag thin film can be obtained [Fig. 3(c)]. With $\epsilon_m = 1.0$ (complete air) and $\epsilon_m = 2.13$ (complete SiO₂), the LSPR peaks of the defined composites are 431 and 433 nm, respectively. However, the result indicates that the calculated LSPR peak is not as good as that of the foregoing mixture model.

In contrast with the above consideration of an effective single uniform particle, we construct another effective geometric structure, that is, an effective core–shell model, to describe the SiO₂@Ag nanoparticle, as can be seen in Fig. 3(a) (iii).^{26,28} We consider the Ag nanoparticles (or SiO₂) as the core and an effective medium layer (EML) of SiO₂ and air (or Ag and air) as the shell. Figure 3(d) shows the fitted curves with an Ag core and a SiO₂ core, respectively, for the SiO₂@Ag thin film. In the case of the Ag core, the fitted curve with a medium of $\epsilon_m = 1.0$ (complete air) and $\epsilon_m = 2.13$ (complete SiO₂) represents LSPR peaks at 418 and 430 nm, respectively. The Ag core–shell has an approximate shell thickness of 1.33 nm and Ag nanoparticles of a similar size. The calculated spectrum of Core_{Ag}–EML shows a better fit than that of Core_{SiO₂}–EML.

According to the results calculated by different models, the classical Mie theory is the simplest and the most direct theory to model the optical behavior of the thin-film SiO₂@Ag. However, the optical behavior of SiO₂@Ag thin film can only be described well by using a mixture of both the calculated spectrum of Ag nanoparticles and the experimentally determined spectrum of SiO₂ nanocarriers. That is to say, the spectral fitting revealed that the impact of the surrounding environment is relatively fundamental. We can hardly achieve a precise calculation of the spectrum through a single step modeling. In other words, the EMT merges all the factors of the surrounding environment as an effective dielectric function for the calculations, while the final model considers the

environment around the Ag nanoparticles as an effective shell structure. This gives rise to a more precise prediction of the experimental spectrum. In addition, this model can be applied with various filling factors or shell thicknesses of EML, allowing a vast number of synthetic parameters to be manipulated for a variety of potential sensing purposes.

In conclusion, the SiO₂@Ag satellite nanoparticles deposited on the glass substrate were prepared and applied as transparent solid-state optical nanosensors for the detection of melamine molecules. Sensing responsiveness and sensitivity were significantly improved by a factor of 2–4 with respect to the model molecule, melamine, compared with the liquid-state version of the sensors, indicating that a strong dielectric interference occurred when the latter were used. By using the classic Mie theory and EMT, we proposed three featured models for the calculation of LSPR spectra of solid-state SiO₂@Ag thin films, and the resulting valuable data from a combination of classic Mie model fitting and a measured SiO₂ spectrum allowed precise prediction using the realistic solid-state SiO₂@Ag thin film chemical sensor which is technically feasible for practical uses.

¹A. Moores and F. Goettmann, *New J. Chem.* **30**, 1121 (2006).

²S. K. Ghosh and T. Pal, *Chem. Rev.* **107**, 4797 (2007).

³C. Noguez, *J. Phys. Chem. C* **111**, 3806 (2007).

⁴Z. Q. Tian, B. Ren, and D. Y. Wu, *J. Phys. Chem. B* **106**, 9463 (2002).

⁵D. Graham, K. Faulds, and W. E. Smith, *Chem. Commun.* **2006**, 4363.

⁶W. P. Hu, S. J. Chen, K. T. Huang, J. H. Hsu, W. Y. Chen, G. L. Chang, and K. A. Lai, *Biosens. Bioelectron.* **19**, 1465 (2004).

⁷S. D. Soelberg, T. Chinowsky, G. Geiss, C. B. Spinelli, R. Stevens, S. Near, P. Kauffman, S. Yee, and C. E. Furlong, *J. Ind. Microbiol. Biotechnol.* **32**, 669 (2005).

⁸A. Ramanavičius, F. W. Herberg, S. Hutschenreiter, B. Zimmermann, I. Lapėnaitė, A. Kaušaitė, A. Finkelšteinas, and A. Ramanavičienė, *Acta Med. Lituanica.* **12**, 1 (2005).

⁹W. Sritravanich, N. Fang, C. Sun, Q. Luo, and X. Zhang, *Nano Lett.* **4**, 1085 (2004).

¹⁰X. Wei, X. Luo, X. Dong, and C. Du, *Opt. Express* **15**, 14177 (2007).

¹¹K. Tanaka and M. Tanaka, *Opt. Express* **14**, 10603 (2006).

¹²R. Vogelgesang, J. Dorfmueller, R. Esteban, R. T. Weitz, A. Dmitriev, and K. Kern, *Phys. Stat. Sol. B* **245**, 2255 (2008).

¹³S. P. Mohanty and E. Kougianos, *IEEE Potentials* **25**, 35 (2006).

¹⁴B. Sepúlveda, P. C. Angelomé, L. M. Lechuga, and L. M. Liz-Marzán, *Nano Today* **4**, 244 (2009).

¹⁵L. Gunnarsson, T. Rindzevicius, J. Prikulis, B. Kasemo, and M. Käll, *J. Phys. Chem. B* **109**, 1079 (2005).

¹⁶N. Nath and A. Chilkoti, *J. Fluoresc.* **14**, 377 (2004).

¹⁷F. Frederix, J. M. Friedt, K. H. Choi, W. Laureyn, A. Campitelli, D. Mondelaers, G. Maes, and G. Borghs, *Anal. Chem.* **75**, 6894 (2003).

¹⁸T. Endo, R. Ikeda, Y. Yanagida, and T. Hatsuzawa, *Anal. Chim. Acta* **611**, 205 (2008).

¹⁹C. Han and H. Li, *Analyst* **135**, 583 (2010).

²⁰H. Li, F. Li, C. Han, Z. Cui, G. Xie, and A. Zhang, *Sensor Actuat. B* **145**, 194 (2010).

²¹T. Matsushita, T. Nishikawa, H. Yamashita, R. Hasui, S. Fujita, and Y. Okuno, *Jpn. J. Appl. Phys.* **47**, 7420 (2008).

²²J. Zhao, X. Zhang, C. R. Yonzon, A. J. Haes, and R. P. Van Duyne, *Nanomedicine* **1**, 219 (2006).

²³R. Gradess, R. Abargues, A. Habbou, J. Canet-Ferrer, E. Pedrueza, A. Russell, J. L. Valdés, and J. P. Martínez-Pastor, *J. Mater. Chem.* **19**, 9233 (2009).

²⁴R. D. Jean, K. C. Chiu, T. H. Chen, C. H. Chen, and D. M. Liu, *J. Phys. Chem. C* **114**, 15633 (2010).

²⁵C. F. Bohren and D. R. Huffman, *Absorption and Scattering of Light by Small Particles* (Wiley, 1998).

²⁶See supplementary material at <http://dx.doi.org/10.1063/1.4722583> for theoretical formulas.

²⁷G. A. Niklasson, C. G. Granqvist, and O. Hunderi, *Appl. Opt.* **20**, 26 (1981).

²⁸J. Zhu, *Physica E* **27**, 296 (2005).